Gamma ray spectroscopy with Arduino UNO

C. M. Lavelle

Citation: American Journal of Physics **86**, 384 (2018); doi: 10.1119/1.5026595
View online: https://doi.org/10.1119/1.5026595
View Table of Contents: http://aapt.scitation.org/toc/ajp/86/5
Published by the American Association of Physics Teachers

CrossMark click for updates

APPARATUS AND DEMONSTRATION NOTES

The downloaded PDF for any Note in this section contains all the Notes in this section.

John Essick, *Editor*
Department of Physics, Reed College, Portland, OR 97202

This department welcomes brief communications reporting new demonstrations, laboratory equipment, techniques, or materials of interest to teachers of physics. Notes on new applications of older apparatus, measurements supplementing data supplied by manufacturers, information which, while not new, is not generally known, procurement information, and news about apparatus under development may be suitable for publication in this section. Neither the *American Journal of Physics* nor the Editors assume responsibility for the correctness of the information presented.

Manuscripts should be submitted using the web-based system that can be accessed via the *American Journal of Physics* home page, http://ajp.dickinson.edu and will be forwarded to the ADN editor for consideration.

Gamma ray spectroscopy with Arduino UNO

C. M. Lavelle[a)]
Applied Physics Laboratory, The Johns Hopkins University, Laurel, Maryland 20723

(Received 30 October 2017; accepted 14 February 2018)

We review a simple gamma ray spectrometer constructed on a solderless breadboard. The spectrometer's detector consists of a CsI(Tl) scintillator and silicon photomultiplier (SiPM) and its readout is facilitated by an Arduino UNO. The system is low cost and utilizes a minimum of components while still achieving satisfactory charge linearity and noise levels. This instrument can be used in instructional laboratories to introduce both radiation detection and analog signal processing concepts. We also expect it will be of interest to those seeking to introduce gamma spectroscopy to the expanding ecosystem of Arduino hardware. © *2018 American Association of Physics Teachers.*
https://doi.org/10.1119/1.5026595

I. INTRODUCTION

A. Motivation

Detection of ionizing radiation lies at the heart of nuclear physics. Nevertheless, implementation of the required spectroscopy system in an instructional laboratory is typically an expensive undertaking. We demonstrate a simple, low-cost gamma ray spectrometer, which takes less than an hour to assemble on a solderless breadboard, making it ideal for educational use. Analog readout, amplifier and detector bias supply voltages, histogram data storage, and logic control signals are carried out using the popular Arduino UNO microcontroller,[1] augmented by a commercial Arduino expansion board.

Our primary aim is to provide a convenient introduction to scintillation spectroscopy for the student laboratory. However, there is also broader interest in low cost, widely distributable medium energy-resolution gamma ray spectroscopy for security applications[2,3] as well as efforts in "citizen-science" environmental monitoring in the wake of the Fukushima incident.[4] The simple approach to spectroscopy demonstrated here has potential to evolve into a much more capable instrument that could support these non-academic activities if combined with the other capabilities present in the Arduino ecosystem. These capabilities include many easy-to-use hardware components such as GPS, touch screen displays, additional sensors, and data storage devices, and, most importantly, the vibrant user community.

B. Overview

In scintillation spectroscopy,[5–7] the energy spectrum of a gamma ray field is measured by converting the gamma rays into visible light pulses in a scintillator material. The light pulses are observed by a low-level light detector attached to the scintillator. Common choices for the detector include a photomultiplier tube (PMT), avalanche photodiode (APD), or most recently, silicon photomultiplier (SiPM).[8]

The light emission in the scintillator decays over a time scale that is characteristic of the particular material employed, ranging from tens of ns to several μs. In our setup, this light pulse is detected by a SiPM and a charge sensitive preamplifer (CSP) is used to integrate the resulting current pulse from this light detector into a voltage pulse. The CSP voltage pulse height is proportional to the total photoelectron induced charge emitted by the SiPM. In this way, the CSP pulse height provides a measure of the ionization energy deposited in the scintillator by the gamma ray.

Analog or digital processing methods can be employed to measure the CSP pulse height. Analog signal processing improves the signal-to-noise ratio by the application of a Gaussian shaping amplifier to the CSP signal before the pulse height is measured. The shaping amplifier acts as both a bandwidth filter and a signal amplifier. It also removes the long tail from the preamplifier output to alleviate pulse-pileup between nearby events in time.

Digital signal processing (DSP) methods record the output of the CSP using a high speed analog-to-digital converter (ADC) with sampling rates on the order of 50,000 samples per second (S/s). DSP convolutes the measured CSP signal with a trapezoidal filter; the rise time of the trapezoid is analogous to the shaping time of an analog shaping amplifier. However, an advantage of DSP is that it retains good resolution at relatively high throughput.[5] In another digital approach, the light

 © 2018 American Association of Physics Teachers

detector's output is digitized directly at even higher rates (>250 MS/s). High-rate digitization is used when temporal pulse shape information is desirable such as in pulse shape discrimination.[5,9]

The Arduino UNO is based on the ATmega328p microcontroller and has an ADC sampling rate is on the order of ~10 kS/s. This slow sampling time compared to the light pulse width means the analog pulse height cannot be directly measured accurately. The sampling is also too sparse to support the DSP method.

The solution in this case is to employ a "peak detector," a classic analog circuit that allows the conversion of transient voltage pulse heights into persistent voltages. We employ a peak detector integrated circuit (PDIC) to hold the voltage pulse height in analog memory until it can be read by an ADC on, or controlled by, the Arduino. A similar approach is taken by the ArduSiPM,[10] a recently developed muon cosmic ray detector,[11] and high channel density SiPM readout application specific integrated circuits (ASICs).[12,13]

This paper is organized as follows. The individual components of the system and some of the underlying physics are addressed in Sec. II. Section III shows the results of a charge calibration, example gamma ray spectra, and an energy calibration. Results with this apparatus are then shown to compare favorably to readout using standard Nuclear Instrumentation Modules (NIM). Finally, we discuss and demonstrate a few possible experiments that may be conducted in Sec. IV and present an outlook for this research in Sec. V.

II. SYSTEM COMPONENTS

The general features of our circuit are shown in Fig. 1. The SiPM is biased using a positive high-voltage supply and AC coupled through a blocking capacitor to the charge sensitive preamplifier (CSP). The CSP is AC coupled to the PDIC, which is controlled and read out by the Arduino microcontroller. A brief description of each component follows, beginning with the scintillator and working through the analog signal chain.

A. Scintillator, SiPM, and bias

The design choices surrounding scintillator material, SiPM, and SiPM bias module are tightly interconnected. We employ polished blank CsI(Tl) crystals procured from Alpha Spectra and Saint-Gobain with dimensions of 6 mm × 6 mm × 50 mm and wrapped with 4 layers of BC-642 PTFE Reflector Tape from Saint-Gobain. The scintillator is coupled to the SiPM

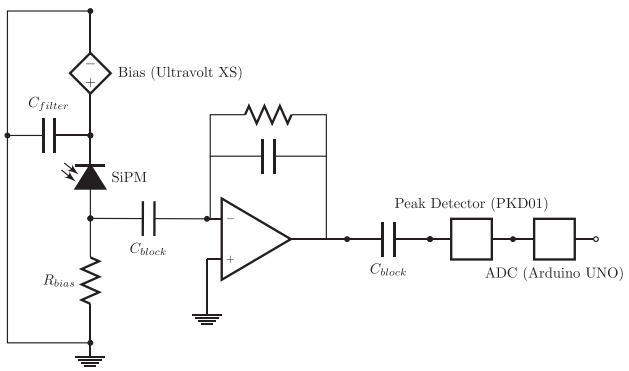

Fig. 1. Basic circuit diagram, showing bias, SiPM, charge sensitive preamplifier, peak and hold IC and microcontroller based ADC.

using Alpha Spectra optical silicone grease. Some care must be taken to ensure that the PTFE does not contact the silicone grease, which results in degraded performance of the PTFE.

CsI(Tl) is chosen because it has a high light yield of 40–60 photons per keV of deposited energy[14] and sufficient energy resolution. The emission wavelength peaks at around 550 nm; according to manufacturer specifications, the SiPM is about 15% efficient at this wavelength. Combined with the high gain of the SiPM, the signals are sufficiently large to be easily measured. CsI(Tl) is also less hygroscopic than other scintillators such as NaI(Tl), so that it can be handled (with latex gloves) without the need for hermetic encapsulation. The crystal is stored in a dry box when not in use because it will degrade over long periods if humidity is allowed to attack its surface.[15]

The dimensions were initially chosen to match the SiPM area and provide good stopping power for a directly incident ^{137}Cs gamma ray at 661 keV on the long axis of the crystal. However, the implications of this geometry are notable. The ratio of the total counts to the counts in the photopeak to the total number of counts is the peak-to-total ratio. If the crystal width is small compared to the mean free path of secondary scattered particles, then these secondaries can escape without contributing to the photopeak.[5] The end result is a low peak-to-total ratio that varies strongly based on the relative orientation of the crystal and source. A long rod such as this may degrade energy resolution.[16] It has been found that light collection may be improved if the crystal is slightly smaller in area than the SiPM active area so that light escape at the edges is avoided.[17]

SiPM can be used with larger scintillators to increase the gamma ray detection efficiency, but often only a fraction of the scintillator face is observed by the light detector. In this case, the amount of detected light is also reduced. This reduction in light collection tends to broaden the energy resolution as the statistics of light collection are degraded. Multiple SiPM can be used over the crystal face and summed to a single signal, but the total cost in doing so can exceed that of a large area PMT. However, it has been shown that good resolution can be obtained even if the area is not completely covered, especially if the SiPMs are judiciously placed.[18]

We have employed the SMPTA version of the 6 mm × 6 mm SENSL MicroFC-60035 SiPM, which is attached to a printed circuit board (PCB) for ready insertion into a prototyping board or IC socket. One can also hand solder the connections to a SiPM, which we have found to give similar results. The SiPM high-voltage (HV) bias is supplied by a positive output Ultravolt XS series programmable high-voltage power supply. The HV output is varied from 0 V to 100 V by an analog input signal between 0 V and 2.5 V.

A SiPM is an array of reverse-biased single photon avalanche photodiodes (SPADs), each in series with a quench resistor. In our MircoFC-60035 unit, each SPAD is 35 μm across. The SPADs are biased to just over their breakdown voltage. In this state, the SPADs act as a kind of switch, producing a burst of charge when struck by a photon. SiPM gain at a nominal overvoltage of 2.5 V is typically on the order of 10^6 emitted electrons (~0.5 pC) per detected photon.

There are some considerations that accompany SiPM use. SiPM gain varies considerably with temperature, e.g., on the order of 1% per degree C for the MicroFC-60035. SiPMs also suffer from correlated noise terms (cross-talk and afterpulsing) and high dark pulse rates (28 kHz mm^{-2}). Finally, each SPAD has a reset time defined by the *RC* constant of

the quench resistor (95 ns). If a second photon strikes the SPAD during the reset time, then this photon will not be detected. If the number of photons in the pulse is comparable to the total number of SPADs in the SiPM and those photons arrive in a short burst, then a non-linear response is possible.[19] The CsI(Tl) crystal, while relatively bright, emits over a pulse width of several μs. This pulse width is much longer than the $\sim$200 ns recovery time of the SPAD. The difference in time scales of recovery and incident light pulse width, taken together with the 18,980 SPADs on the SiPM, minimizes the potential for non-linearity in this experiment.

A variable HV supply is chosen because SiPM gain, dark current, cross-talk probability, and after-pulsing rates all vary with applied bias. The gain and correlated noise terms impact the optimal energy resolution that can be achieved. A programmable HV source therefore facilitates parametric studies of SiPM response as a function of bias. It also provides a ready means to implement microcontroller-directed feedback to stabilize the SiPM gain against changes in temperature.

B. Analog readout

The CSP is a low-cost hybrid circuit preamplifier module (Cremat CR-113) with a specified pulse height sensitivity of 1.3 mV pC^{-1} and decay time of 50 μs. The preamplifier is often followed by a *CR* – *RC* Gaussian shaping amplifier, however, in this system a shaping amplifier is not used for several reasons. Foremost, we seek to minimize the total number of components. Shaping amplifiers often require pole adjustment compensation and baseline restoration circuitry. This adds unnecessary complexity to the project because the high SiPM gain produces a CSP output that can be measured without further amplification. Electronic noise will be shown later to be acceptable. Additionally, the scintillator is small so the event rate is low. The overlap of preamplifier decay tails is therefore infrequent.

Nevertheless, if the event rate is on the order of, or greater than, the pulse processing time ($\sim$150 μs), distortion of the measured spectrum is possible. A CSP with a longer decay time may also not be suitable. We have not yet developed a dead time model for this system, but it would be influenced by the readout averaging time and managing communication between the Arduino and any other devices such as the computer or serial port.

The peak detection functionality is provided by a conveniently packaged IC (Analog Devices PKD01). It is biased to 7 V to cover the full 3 V dynamic range of the CSP and set for unity gain inverting operation according to the datasheet. Unfortunately, this component is obsolete and no longer produced by the manufacturer. It can still be obtained through, for example, authorized obsolete parts vendors or eBay. Another option is to construct a peak detector circuit using a few op amps.[20] Many major manufacturers list peak detector circuit designs in the applications sections of the op amp datasheets, e.g., Analog Devices AD8034.[21,22] A voltage-controlled switch to ground can be added to the basic design to reset the hold capacitor.

C. Arduino UNO components

There are several demands on the microcontroller and other supporting components. We desire high precision measurement of the peak signal held by the PDIC. Additionally, $\sim$mV level analog temperature measurement and constant output control voltage to the programmable HV is required for SiPM temperature stabilization. In comparison, the Arduino UNO analog out is not constant, but rather a pulse width modulated (PWM) signal from select digital pins. Finally, the HV supply requires +5 V power and the CSP and PKD01 share the $\pm$7 V (or greater) bias supply.

These requirements are met by the Digilent Analog Shield (DAS) prototyping extension board for the Arduino UNO. This low-cost "shield" (as these extensions are known) contains 4 channels each of 16-bit ADC and DAC communicating over the SPI bus as well as a fixed $\pm$5 V and an adjustable voltage supply up to $\pm$7.5 V. Twisted pairs are used to conduct signals from the DAS to the solderless breadboard.

Table I. Cost of components.

Item	Model	Cost
CsI(Tl) Scintillator	Alpha Spectra	\$150
Silicon Photomulitplier	SENSL MicroFC-SMTPA-60035 (PCB)	\$160
	SENSL MicroFC-60035-SMT (bare die)	\$60
HV	ULTRAVOLT XS	\$100
Charge Sensitive Preamplifier	CREMAT CR-113	\$50
Peak Detector IC	Analog Devices PKD01	\$10 (ebay)
ADC/DAC	DIGILENT Analog Shield	\$50
Data Acquisition	Arduino UNO	\$30

The component costs are detailed in Table I. The cost of the total system as pictured is \$550. There are several ways in which costs can be lowered. Smaller scintillators can be ordered in bulk or lower cost crystals can be used. The programmable power supply can be replaced with a battery or fixed voltage DC-DC converter. A smaller scintillator will utilize a smaller SiPM as well, further reducing costs. SiPM can often be purchased as bare die elements at a bulk discount. Therefore, we estimate construction of the circuit can be reduced to less than \$300, if desired.

D. Operation and Arduino program

The circuit "hook-up" diagram is shown in Fig. 2 and the completed apparatus is shown in Fig. 3. The HV output has

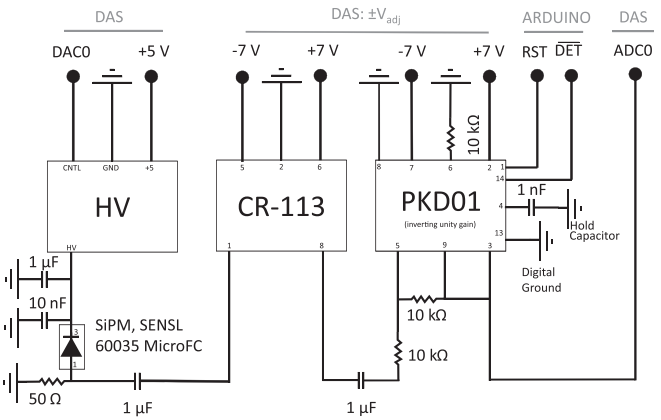

Fig. 2. Connections within the breadboard to the components are shown. External connections to the ARUDINO UNO logic pins and Digilent Analog Shield (DAS) are shown across the top.

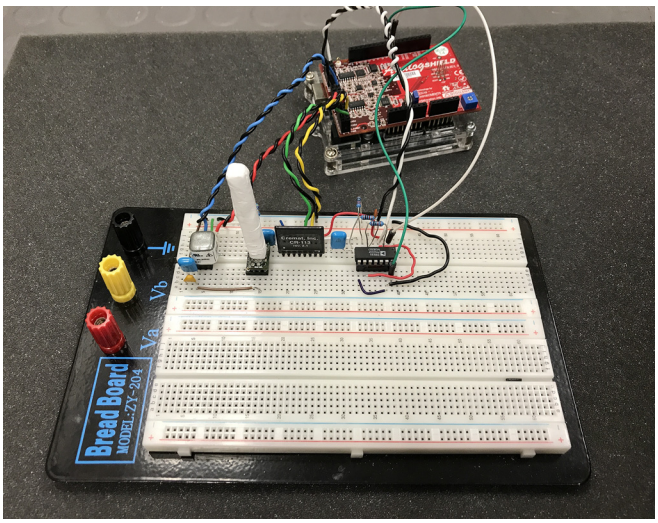

Fig. 3. The completed apparatus.

1 μF and 10 nF smoothing capacitors in parallel to reduce HV ripple. The measured ripple was 70 mVpp on the breadboard. This high value is not unexpected for a breadboard environment, but it is still much higher than the 10 mV level specified for this component. Nevertheless, the given HV output is sufficient for these measurements because the ripple must only be small compared to the ~2.5 V SiPM overvoltage to minimize its impact on measured result.

In addition, a 50 Ω bias resistor is connected between the SiPM output and ground and a 1 μF decoupling capacitor is connected from the SiPM to the CSP. The high dark current (~1 μA) of the SiPM would lead to a DC offset in the output of the CR-113, so a 1 μF decoupling capacitor connects the CSP output to the PDIC.

The PDIC logic for detection ($\overline{\text{DET}}$) and reset (RST) is controlled on separate logic pins connected to the Arduino UNO. Some care must be taken to ensure that the logic pins chosen for the PDIC control are not shared by other devices and are free from pickup noise on neighboring pins or the serial bus. Finally, the DAS connects to the HV control voltage and PDIC output; it also provides power to the HV, preamplifier, and PDIC.

The system is programmed using the Arduino Software (IDE, v1.2.16) and libraries supplied by the DAS manufacturer. The PDIC is initialized in a tracking state by setting its RST and $\overline{\text{DET}}$ pins to the low logic state. There is no discriminator. Instead, the ADC repeatedly measures the PDIC output voltage. If the voltage is measured to be above a lower-level noise threshold, set in the Arduino program (or "sketch") at ~35 mV, then $\overline{\text{DET}}$ is set to high such that the PDIC input is no longer tracked and the current value is held in "analog memory."

The CSP must rise to its full value, integrating the entire scintillation pulse, before tracking is disabled. Fortunately, the rise time is fast enough compared to the Arduino clock speed that no delays are necessary. However, faster microcontrollers or slower charge collection times may require adding a delay before $\overline{\text{DET}}$ is set to high. The benefit to disabling tracking shortly after pulse detection is that subsequent pulses that would be distorted by the previous pulse's long tail are ignored.

The Arduino then waits 45 μs (the settling time of the PDK01) before averaging the result of 5 measurements of the PDIC output to measure the pulse height. The PDIC is then reset to baseline by setting the RST pin to logic high for 15 μs to allow the capacitor to fully discharge. After the discharge is complete, RST and $\overline{\text{DET}}$ are reset to logic low and the measurement cycle repeats. Scope traces showing the SiPM, CSP, and peak and hold output for one event are shown in Fig. 4.

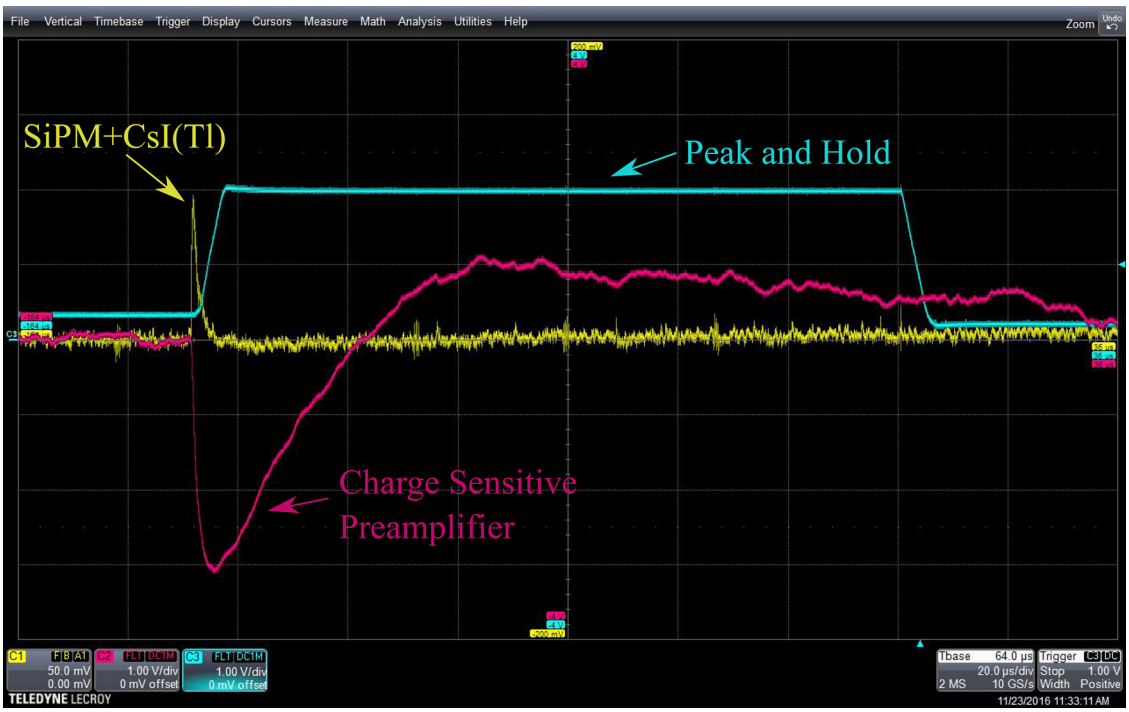

Fig. 4. Scope trace created using 1 MΩ probes representing the SiPM output signal (taken at the CSP input after the decoupling capacitor), the CSP output pin, and the peak and hold output pin.

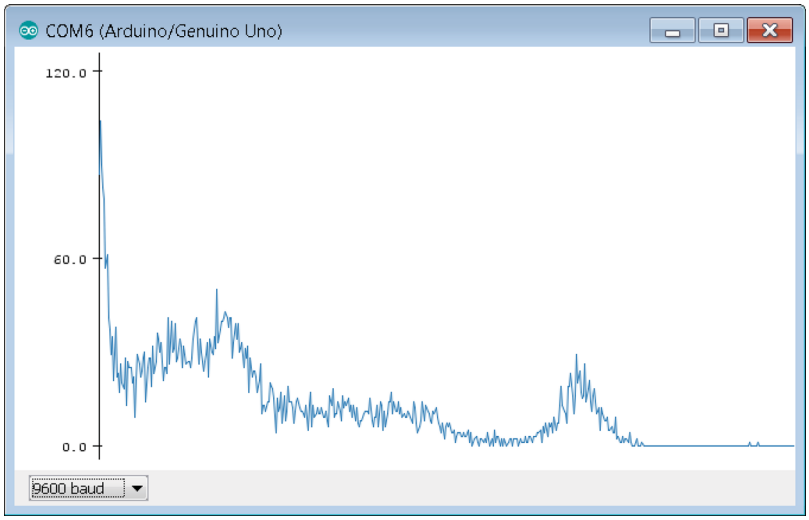

Fig. 5. A developing spectrum viewed in the Arduino Serial Plotter.

The gamma ray spectrum is created from the measured CSP pulse height using a 512-element integer array, limited to roughly this size by the remaining standard SRAM Arduino memory. The array index corresponding to the pulse height is determined directly from the 16-bit unsigned integer ADC output by scaling the positive side of the 5 V range to ~2.5 V dynamic range of the CSP over 512 channels. This is accomplished using the following equation:

$$ArrayIndex = \mathbf{floor}\left(\frac{ADC - 2^{15}}{32}\right). \quad (1)$$

The indicated array index is then incremented by one and the system resets. *ArrayIndex* must be conditioned to avoid terms that are less than 0 and greater than 512. Indexing an illegal array location (segmentation fault) was observed to cause unpredictable behavior such as causing the Arduino to reset.

Experiments are conducted by placing the entire Arduino system in a dark box and passing the USB connection to the cable through the box bulkhead. Any exposed LEDs on the Arduino components should be masked. Additionally, exposure of the crystal to UV light (such as from fluorescent lamps) should be minimized. The excitation of long-lived phosphorescence in CsI(Tl)[23] will negatively impact resolution.

There are several ways to view the data. The Arduino IDE provides a rudimentary plotting capability. The plotter displays up to 500 data points if the data are output to the serial port in the proper format, but axis labels are absent. An example ^{137}Cs spectrum observed using the serial plotter is shown in Fig. 5.

The Arduino can also print the 512-element array to the serial port at regular intervals (every 1000 events or 10 s, whichever comes first). For the remainder of this paper, the presented data are simply cut-and-pasted from the IDE's serial port monitor to a text file for offline analysis and plotting in MATLAB.

III. RESULTS

A. Linearity and electronic noise measurement

A key question regarding our spectrometer was whether operation on a solderless breadboard introduced excess noise, either from stray RF or coupling between the terminals of the board. To establish our system's charge linearity, calibration, and electronic noise, a Berkeley Nucleonics Corporation DB2 tail pulse generator was used to input a step voltage (V_{step}) into a known capacitor mounted in a BNC Pomona box. The tail was set to 1 ms with the fastest rise time of 100 ns. An oscilloscope (1 MΩ input impedance) was connected in parallel with the capacitor in order to monitor the step voltage.

The test capacitor's value, $C_{test} = 512 \pm 4$ pF, was measured by observing the *RC* decay time when placed in series with a 4.3 kΩ resistor. Uncertainty was dominated by the propagated error in the resistance (measured by multimeter) and 1-σ statistical fluctuation of the fall time measured by the digital oscilloscope built-in measurement features (LeCroy WR640Zi). The result was consistent with the 500 pF capacitor used (5% tolerance) and RG58 connecting cable capacitance.

The capacitor box was connected to the input of the CSP on the breadboard after the SiPM was removed. The charge Q input into the system is given by

$$Q = C_{test}V_{step}. \quad (2)$$

Results of the charge calibration are shown in Fig. 6. The result is satisfactorily fit to a linear function. A second-order

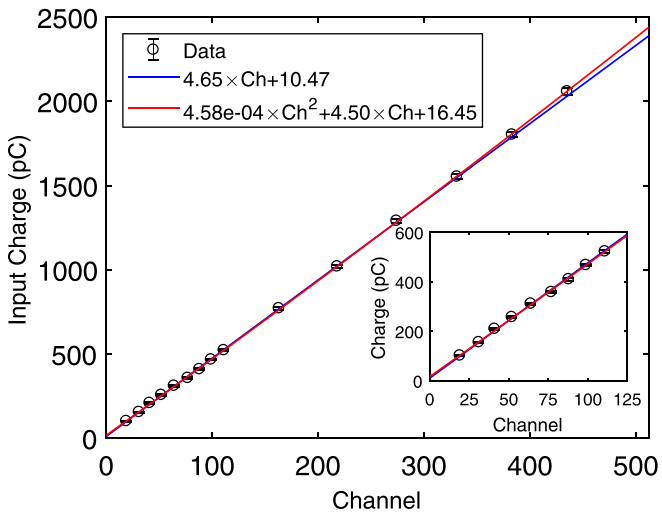

Fig. 6. Results of charge calibration, showing satisfactory linearity.

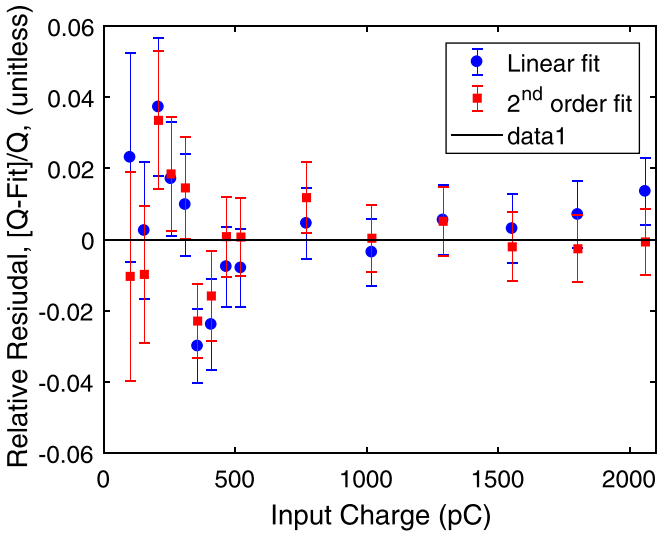

Fig. 7. Relative residuals of the fit in Fig. 6. The system has less than 4% non-linearity through the dynamic range.

polynomial fit is also shown for comparison. The relative residuals to each fit are shown in Fig. 7. The linear fit is sufficient for the present work, but the system appears slightly non-linear as the CSP nears the specified saturation input charge of 2100 pC. There is also a slight non-linearity near 200 pC. The non-linearity, defined as

$$Non-Linearity = \frac{Q_{meas} - Q_{fit}}{Q_{meas}} \times 100\%, \quad (3)$$

is better than 4% throughout. For comparison, a similar test of the standard nuclear instrumentation showed less than 2% non-linearity below 500 pC and less than 0.5% for larger charge pulses.

Finally, the width of the pulses in channel space provides a measure of the instrumental noise. We find ∼2 channel full width at half maximum (FWHM), corresponding to about 12 mV, on all test pulses across the dynamic range. Results

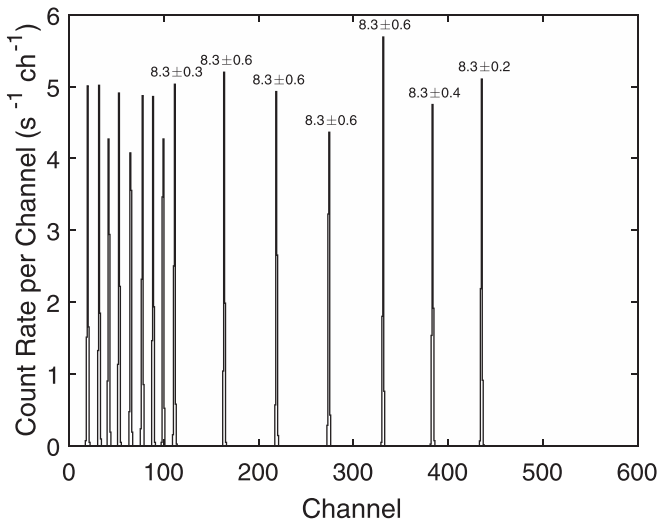

Fig. 8. Full dynamic range noise test. Each peak is normalized to its rate, such that if the width was 1 channel wider it would appear shorter than its neighbors. The count rate (s^{-1}) is shown above each peak.

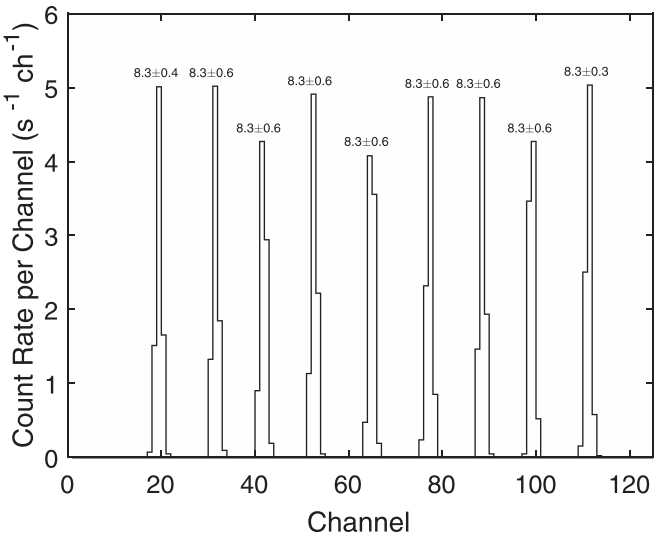

Fig. 9. Low charge dynamic range noise test. The count rate (s^{-1}) is shown above each peak.

of this noise test are shown for the full dynamic range in Fig. 8 and at low charge in Fig. 9. Each point is normalized by the pulse rate, which is a consistent 8.3 pulses per second for all measurements.

B. Energy calibration

Calibration of the CsI(Tl) crystal from Saint-Gobain was performed using a 10 μCi (370 kBq) calibration source set from Eckert and Zeigler (GF-290-10D), comprised of a number of gamma ray sources that emit at the energies shown in Table II. The SiPM is biased at ∼27.5 V for all measurements. Peak location was determined by fitting with a Gaussian and linear background term. A two-Gaussian fit was used for the nearby peaks in ^{133}Ba (31 keV and 81 keV, 302 keV and 356 keV), ^{60}Co, and to separate the 122 keV gamma ray in ^{57}Co from the low energy shoulder.

The collected spectra are shown in Fig. 10. Dwell time was also recorded by the Arduino, and no background subtraction has been performed. Low peak-to-total ratios are observed, especially at higher energy. As such, the ^{60}Co peaks are somewhat difficult to resolve, but easily fit with a two-Gaussian term.

The photopeaks are plotted as a function of channel in Fig. 11. The photopeak energy is linear in channel, indicating that saturation of the SiPM is not occurring. The slight

Table II. Calibration energies and activity on the date of measurement. Uncertainty is the propagated uncertainty of the half-life and ∼3% uncertainty from the source manufacturer (90% confidence level) (Ref. 32). The measurement dwell time for the spectra shown in Fig. 10 are also shown.

Isotope	activity (kBq)	Energies (keV)	Dwell (min)
^{109}Cd	150 ± 8	22, 88	11.5
^{57}Co	86 ± 3	122	21.9
^{133}Ba	345 ± 10	31, 81, 302, 356	16.5
^{22}Na	233 ± 7	511, 1274	40.3
^{137}Cs	368 ± 11	32, 661	79.5
^{54}Mn	96 ± 3	835	53.5
^{60}Co	310 ± 9	1173, 1333	66.3

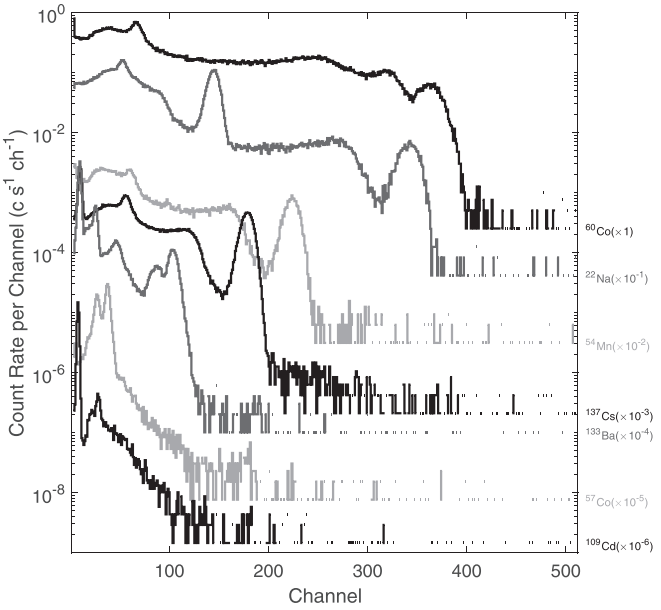

Fig. 10. Measured spectra used for energy calibration.

non-linearity at low energy is expected for CsI(Tl) due to non-proportionality,[17,24,25] but low energy non-linearity observed during the charge calibration is likely also a playing a role.

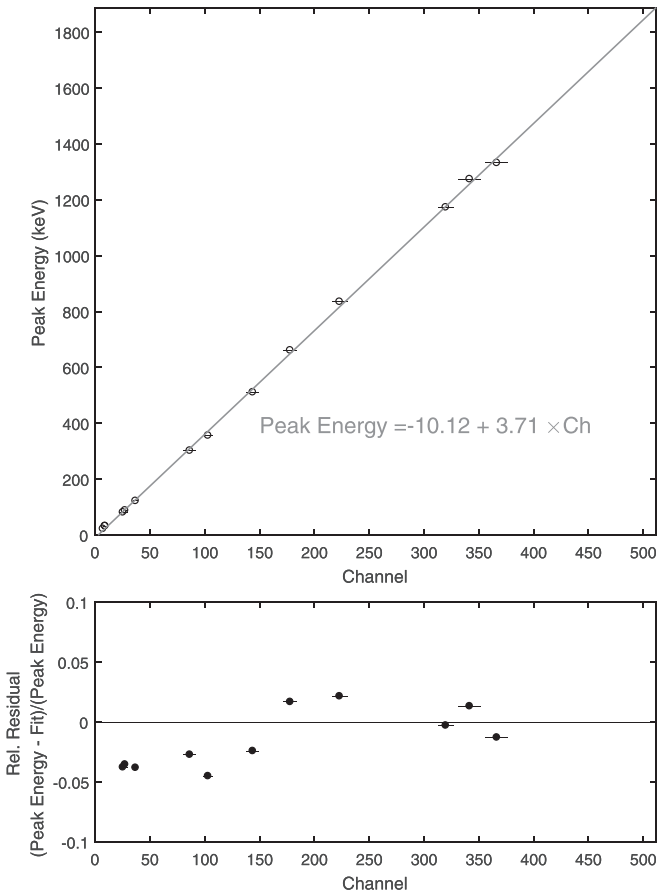

Fig. 11. Energy calibration results, showing satisfactory linearity for the SiPM readout of the CsI(Tl) crystal. Non-linearity at energies below 100 keV may result from low energy non-linearity observed during charge calibration, but is also consistent with expectations for CsI(Tl).

C. Comparison to standard instrumentation

A measurement of ^{137}Cs is shown in Fig. 12 in comparison to standard instrumentation. The standard instrumentation was a CR-Z-SiPM with CR-113 for the CSP, an Ortec 673 shaping amplifier with 6 μs unipolar shaping, and a successive-approximation ADC analog multi-channel analyzer (Ortec Easy MCA). SiPM bias was supplied by BK Precision 9184 bench supply, again at 27.5 V, into an AC coupled signal path on a custom circuit board setup with the two stage bias filter recommended in the SENSL C-series user manual.

The comparison is made using energy calibrated spectra. In the standard instrumentation measurement, the peaks were aligned via a coarse energy calibration based on the 32 keV and 662 keV peaks. A simple linear fit to just two points was sufficient for the coarse energy calibration because we had previously established SiPM linearity. The Arduino spectrum is the same as that shown in Fig. 10 such that the calibration presented in Fig. 11 is used.

Resolution is commonly defined in terms of the full width at half maximum value of the 661 keV peak from ^{137}Cs divided by the peak channel. Typical values for CsI(Tl) range from 5% to 7%, depending on the crystal, geometry, and method of readout.[17] The Arduino system shows a resolution of (8.2 ± 0.2)%, while the standard instrumentation shows (7.8 ± 0.1)%, both at 95% confidence level.

Assuming noise terms add in quadrature, this result is consistent with the previously quantified noise terms for electronic noise (less than 2%) and bias ripple (3%). This measurement also demonstrated a sub-30 keV noise floor.

IV. EXPERIMENTS: BEYOND CALIBRATION

We have demonstrated the basic methods of charge calibration, spectrum measurement, and energy calibration. These experiments represent the necessary steps toward demonstrating sufficient linearity and noise levels for gamma ray spectroscopy. Energy-dependent resolution and efficiency calibrations are obvious next steps.

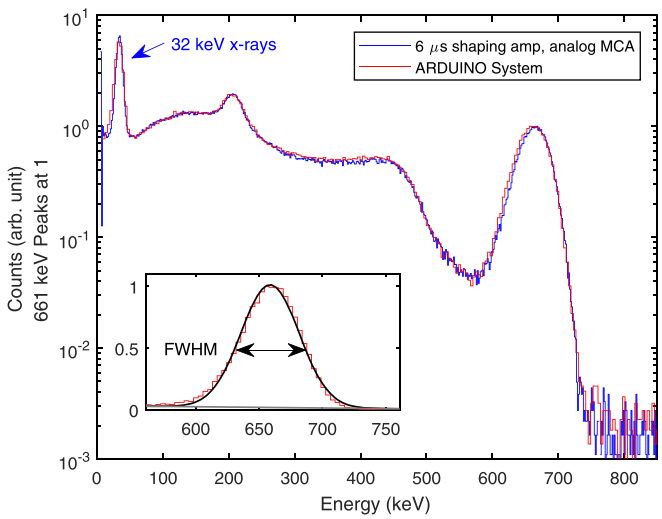

Fig. 12. Comparison of Arduino based readout with high quality nuclear electronics. The 661 keV peaks are normalized to peak at unity. The main differences are a slightly lower noise floor and improved resolution using the standard instrumentation. (Inset) A fit of a Gaussian and linear background term is shown for the Arduino photopeak at 661 keV.

It is also worthwhile to suggest various opportunities for further study. We loosely group the experiments into the following categories,

- Study of SiPM
- Elements of detector design
- Interpretation of gamma spectra
- Coincidence physics
- Applications

A. Study of SiPM

The apparatus presents an opportunity for hands-on study of the SiPM itself. SiPMs are low cost and are not destroyed by exposure to room light, key benefits for classroom experiments compared to a PMT. SiPMs are also likely to play larger roles in the future of nuclear physics instrumentation. In fields where large numbers of channels are needed, such as calorimeter type experiments or PET imaging, this apparatus presents an opportunity to understand the underlying hardware, which is often not directly accessible.

1. Temperature effects

The impact of temperature change can be observed directly using gamma spectral measurements, for example, by gentle external heating of the dark box to slowly increase the SiPM and crystal temperature. Note: Rapid temperature changes can cause the scintillator crystal to fracture. Such heating will cause the photopeak's channel to decrease as the SiPM breakdown voltage increases with increasing temperature.

Temperature fluctuations of just a few degrees Celsius are also sufficient to observe changes in the photopeak position. We have observed day to night variations in our lab. If temperature is simultaneously measured, then the effect can be studied. The Arduino can then be programmed to perform an active correction applied to the bias to compensate for changes in temperature. This correction represents the combined effects of scintillator light yield[26] and SiPM breakdown temperature dependencies.

A more efficient study can be undertaken if a temperature-controlled chamber is available. In this case, an external pulsed light source can provide a constant signal to allow the SiPM gain by itself to be stabilized. The temperature dependence of the scintillator light yield can then be studied.

2. Bias optimization

There is a close relationship between SiPM photon detection efficiency (PDE), gain, correlated noise, and dark rate. All these SiPM characteristics increase with increasing bias, which in turn affect gamma ray energy resolution. As the bias increases the signal amplitude increases, mostly from the increased gain. However, more photons are being detected with increasing PDE and more noise events coincidentally integrated by the CSP as bias increases. If the bias is too high the noise terms begin to degrade resolution.

A plot of resolution as a function of bias can be used to obtain the optimal operating voltage. An example is shown in Fig. 13 for the Alpha Spectra crystal. The resolution was determined from a series of 10 min spectra measuring ^{22}Na. The Arduino automatically increased the HV bias after each spectrum.

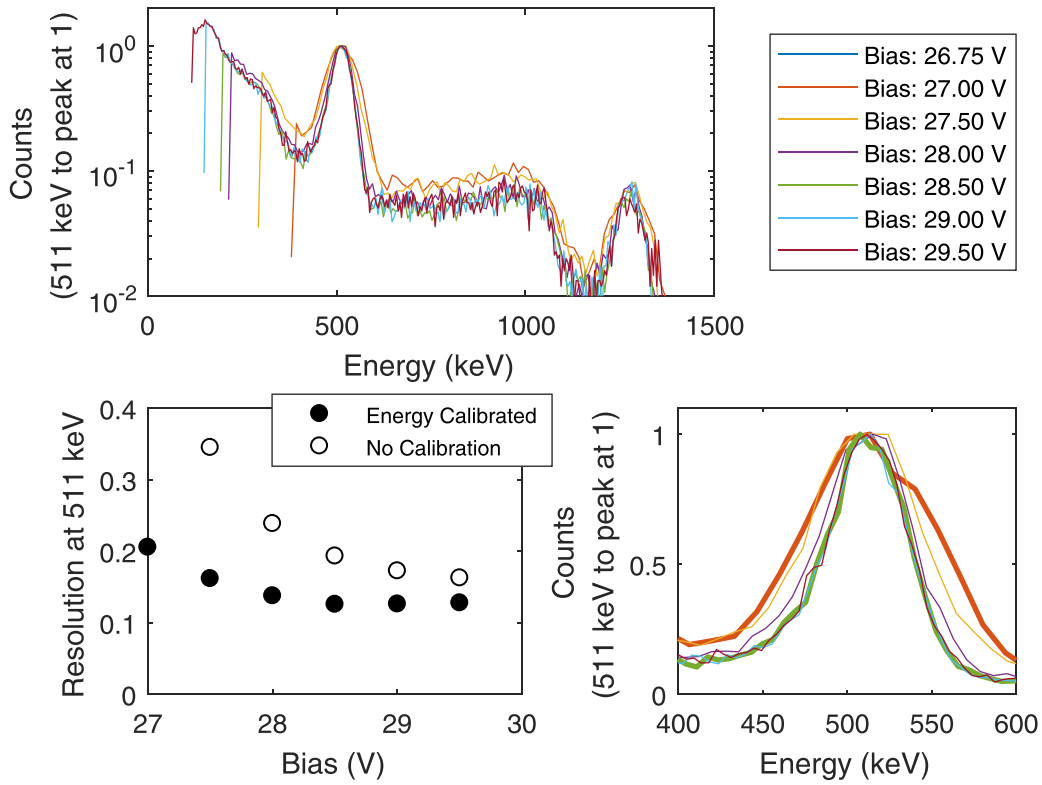

Fig. 13. The Arduino automatically increased the bias in 10 minute intervals for a measurement of ^{22}Na. (Top) Spectra are shown, note the lower limit of detection in energy decreases as bias increases. (Lower, left) Resolution for the 511 keV peak is shown, both calibrated (dark circles) and uncalibrated (white circles) for energy. As bias increases the resolution improves up to to 28.5 V, then gradually degrades. (Lower, right) The 511 keV region is highlighted, with 27 V and 28.5 V shown as the thicker lines for comparison.

For this experiment, ^{22}Na is used because the resolution in energy (not channel) must be established for this measurement. The gain term, α, and offset term β, in the linear calibration are both a function of bias. Thus the fractional energy resolution $\delta E/E$ is given by the following bias-dependent relation:

$$E = \alpha \times Ch + \beta \rightarrow \frac{\delta E}{E} = \frac{\alpha \times \delta Ch}{\alpha \times Ch + \beta}. \quad (4)$$

Resolution in channel space and energy space are only similar if the peak is much larger than the offset, which is not the case when the bias is low. If not energy-corrected, the optimal voltage will erroneously appear to be too large. Figure 13 shows the resolution result in both channel and energy to illustrate this effect.

A two-point calibration is determined for each spectrum and resolution for the 511 keV peak is presented as a function of SiPM bias. At 30 V, the signals are large enough to exceed the dynamic range of the CSP. Equation (1) is essentially a software gain setting, and has to be altered (denominator increased) to accommodate the larger pulses.

B. Elements of detector design

The choice of crystal blanks is deliberate, as it permits study of the optical coupling and reflector. Optical coupling media are used to match the index of refraction between the scintillator and optical window of the SiPM. The student can experiment with using no coupling grease, a silicone pad, or grease to study the impact on signal intensity, peak shape, and energy resolution. Silicone pads require compression for optimal performance, or can be wetted with optical grease if necessary.

Diffuse reflectors such as PTFE are used to eliminate light trapping and improve the uniformity of light collection. The alternative is a specular reflector, such as aluminum foil. The student can try varying these items, and also experiment with eliminating the reflector.

If the radiation source can be collimated and translated along the center axis of the crystal, the position dependence of light collection can be studied. A common medical physics technique is to use a SiPM at each end. By comparing the relative signal intensities, the depth of interaction of the event can be deduced.[27] The type of reflector used is a design consideration in this type of detector, where high position resolution is sometimes more desirable than optimal energy resolution.

Other elements of detector design can also be studied. If multiple lengths of scintillator are available, a study of the effect of crystal aspect ratio (area divided by length) can be undertaken. The ratio of the SiPM area to the area of the SiPM can also be varied, a common consideration in SiPM instrumentation. This can be accomplished without purchasing further scintillators by masking the SiPM and observing the effect on energy resolution.

The student can also change the scintillator used. If the apparatus is charge-calibrated, scintillator non-proportionality can be compared between different materials. Some scintillators also have a significant radioactive background (e.g., LYSO) providing a readily measurable signal as well as an opportunity for background subtraction. A measurement with this apparatus using a PTFE wrapped 4 mm × 4 mm × 22 mm LYSO crystal obtained from eBay is shown in Fig. 14. Plastic scintillator is excellent for charged particle detection[11] and ∼MeV neutron detection via the recoil proton from neutron-hydrogen elastic scattering.

C. Interpretation of gamma spectra

Gamma spectra display a number of features, including the Compton edge and the backscatter peak. The student can use spectroscopy to predict and observe the energy of these events in a calibrated detector. The student can also observe the effect of a high rate by placing the source very close to the detector to attempt to induce pileup peaks.

The relative contributions of the photopeak and Compton continuum can be assessed. In the case of our thin rods, distinctly different peak-to-total ratios are observed when a source is placed above the long axis of the crystal or to its side. Photopeak efficiency itself also changes with source-detector orientation.

The student can also examine the effect of nearby material. Lead (Pb), for example, will emit a 75 keV characteristic X-ray when excited by higher energy sources, such as ^{137}Cs. This is an interesting introduction to not only the physics at work, but also to X-ray florescence (XRF) methods. There are also the common experiments investigating transmission through materials, typically conducted with counting-type apparatus. These experiments can now be conducted in an energy-dependent manner. The buildup of low-energy gamma rays can be separated from the primary radiation and studied as a second aspect of the measurement.

D. Coincidence physics

We have constructed only one example of the apparatus. However, there are three remaining channels on the DAS that can support multiple detectors. This presents the opportunity for the study of coincident events between multiple detectors. In this case, an event in any one detector may initiate readout of all detectors in the apparatus. Time resolution will be limited by the 16 MHz clock on the Arduino UNO, but sub-10 μs resolution should be achievable. Fast analog comparators (there is a free comparator on the PDK01) can also be used for signal coincidence detection to increase time resolution.

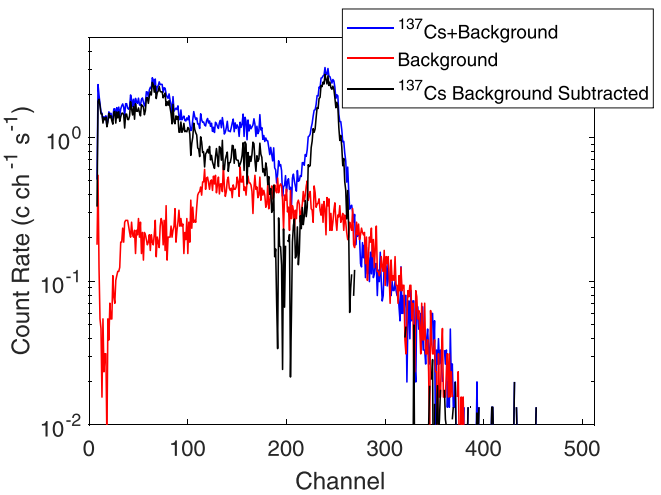

Fig. 14. A ^{137}Cs measurement, replacing the CsI(Tl) with LYSO. Note the intrinsic radioactivity of the ^{176}Lu is clearly observed.

Coincidence can be used in a number of studies. The most straightforward might be to place a ^{22}Na source between two crystals. Coincident events should be 511 keV, but scattering might cause one or both to have a slightly lower energy. In this way, an energy selective-coincidence could be explored.

Coincidence counting is also common in cosmic ray muon detection, which was recently demonstrated in an Arduino-controlled large-area plastic scintillator system.[11] One can also attempt to observe Compton-scattered gamma rays between two scintillators to directly evaluate the Compton scattering energy-angle dependence.

Low background counting methods often utilize anti-coincidence methods to exclude cosmic ray interactions, which would be difficult to implement at low cost. However, beta-gamma coincidence methods are often used in trace radioisotope assays and can be setup using a two channel version of the apparatus presented here.[5]

E. Applications

A number of essential applications have already been discussed, including energy dependent transmission measurements, characteristic X-ray observation, and general aspects of spectroscopic measurement of ionizing radiation. An understanding of these phenomena form the basic skill set needed for health physics (dosimetry and assay), homeland protection (location and identification of unknown samples), materials physics (X-ray and neutron beam techniques), and geology (measurement of radioactive samples).

There are also numerous examples of radioactive goods that can be characterized such as ceramics with uranium containing glazes, dial instruments with radium luminescent paint, thorium welding rods and lantern mantels, industrial smoke detectors with externally measurable quantities of ^{241}Am, and potassium salt substitute. We urge care in procurement of such items, as one must familiarize themselves with applicable laws, internal procedures, and safety considerations.[28] Recent evidence suggests that collections of certain artifacts can increase radon to actionable levels.[29] Antique items should be in good repair, and in some cases (especially smoke detectors), disassembling the device is unlawful.

Finally, there is the possibility of interfacing the device with other capabilities of the Arduino. For example, one might try verifying that background radiation levels often rise with precipitation.[30] For this project, an environmental sensor (temperature, pressure, humidity) and rain sensor or soil moisture gauge could be combined with an SD card shield to log data over long periods of time to attempt to observe this correlation.

Gamma ray backgrounds also vary widely with geographic area. Another application might be to combine the radiation detection with a GPS datalogger, allowing the correlation of background spectra with position.

V. CONCLUSION AND OUTLOOK

We have demonstrated a medium-resolution gamma spectrometer consisting of Arduino hardware, a silicon photomultiplier, an inorganic scintillation crystal, and low-cost analog signal processing components. The Arduino code is straightforward and the application of analog signal processing concepts very direct. The key advantages to this design are primarily pedagogical,[31] however, it also provides a means for introducing scintillation spectroscopy into the Arduino ecosystem. This design is also applicable to any transducer that produces a charge pulse such as a piezoelectric impact sensor.

Our simple approach is similar to other low-cost concepts involving entry level microcontrollers, but is distinguished by its successful achievement of low-noise medium-resolution gamma spectroscopy in the absence of any soldered connections. Only four major electronic components are required on the breadboard (HV, SiPM, CSP, PDIC). The relatively bright CsI(Tl) scintillator[14] and the high gain SiPM produce large, easy-to-measure signals over the electronic noise in the breadboard environment. The Arduino program is also straightforward.[33]

Nevertheless, the thallium in CsI(Tl) is toxic, so laboratory workers should exercise care and review appropriate materials safety data sheets (MSDS) prior to handling. Thallium can be avoided by using CsI(Na) in the same manner. In doing so, we have observed nearly equal performance despite the slightly higher hygroscopic qualities of CsI(Na). The use of plastic scintillator or LYSO may overcome these issues as well, though energy resolution will be degraded.

The next phase of this work will attempt to render the design as a standalone Arduino UNO shield, incorporating a CSP, variable gain Gaussian shaping amplifier, peak detector circuit, bias supplies, high resolution ADC, and temperature sensor.

ACKNOWLEDGMENTS

This project developed over several seasons of the JHU/APL ASPIRE internship program for high school students. Their contributions to this work and enthusiasm for science is appreciated and acknowledged. The initial series of SiPM familiarization studies were carried out together with Priya Kankanhalli from Winters Mill High School in Westminster, Maryland. Early circuit design approaches were explored by Nathan Goonasekeram from Covenant Life School in Gaithersburg, Maryland. Both students are now engaged in university studies, and we look forward to their continued success. Current ASPIRE students Michael Cho, Ben Brown, and Alexandra Herschelman assisted in trial builds of the apparatus as presented in the paper. This work was majority funded by the Internal Research and Development (IRAD) program at JHU/APL. The calibrations undertaken in Sec. III were supported by IRAD funds within the JHU/APL Office of Technology Transfer. Wayne Shanks and Tom Haard are gratefully acknowledged for sharing their expertise through many useful discussions. Fred Olschner of Cremat, Inc. offered valuable advice regarding the CSP and alternative peak detector circuits, which was greatly appreciated. The author also thanks J.C. Fischer and J.M. Kalter for helpful proofreading and technical comments on the manuscript.

[a]Electronic mail: chris.lavelle@jhuapl.edu; Permanent address: 11100 Johns Hopkins Road, Laurel, MD 20723.

[1]Arudino web site, <https://www.arduino.cc>.

[2]DARPA Press Release, "Ushering in a new generation of low-cost, networked, nuclear-radiation detectors," <https://www.darpa.mil/program/sigma https://www.darpa.mil/news-events/2016-08-23>.

[3]D. Ginzburg, Y. Knafo, A. Manor, R. Seif, M. Ghelman, M. Ellenbogen, V. Pushkarsky, Y. Ifergan, N. Semyonov, U. Wengrowicz, T. Mazor, Y. Kadmon, Y. Cohen, and A. Osovizky. "Personal radiation detector at a high technology readiness level that satisfies darpas sn-13-47 and sigma program requirements," Nucl. Instrum. Meth. A **784**, 438–447 (2015).

[4]Azby Brown, Pieter Franken, Sean Bonner, Nick Dolezal, and Joe Moross. "Safecast: successful citizen-science for radiation measurement and communication after Fukushima," J. Radiol. Prot. **36**(2), S82–S101 (2016).
[5]G. F. Knoll, *Radiation Detection and Measurement*, 3rd ed. (John Wiley and Sons, Inc., Hoboken, NJ, 2000).
[6]W. R. Leo, *Techniques for Nuclear and Particle Physics Experiments*, 2nd ed. (Springer-Verlag, Berlin Heidelberg GmbH, 1994).
[7]Gordon Gilmore, *Practical Gamma-ray Spectrometry*, 2nd ed. (John Wiley and Sons, Inc., Chichester, West Sussex, England, 2008).
[8]P. Buzhan, B. Dolgoshein, L. Filatov, A. Ilyin, V. Kantzerov, V. Kaplin, A. Karakash, F. Kayumov, S. Klemin, E. Popova, and S. Smirnov, "Silicon photomultiplier and its possible applications," Nucl. Instrum. Meth. A **504**(13), 48–52 (2003).
[9]Marc Lavi Ruch, Marek Flaska, and Sara A. Pozzi, "Pulse shape discrimination performance of stilbene coupled to low-noise silicon photomultipliers," Nucl. Instrum. Meth. A **793**, 1–5 (2015).
[10]V. Bocci, G. Chiodi, F. Iacoangeli, M. Nuccetelli, and L. Recchia, "The ArduSiPM a compact trasportable [sic] Software/Hardware Data Acquisition system for SiPM detector," in *Proceedings of the 2014 IEEE Nuclear Science Symposium and Medical Imaging Conference (NSS/MIC)*, Seattle, WA (2014), pp. 1–5.
[11]S. N. Axani, J. M. Conrad, and C. Kirby, "The desktop muon detector: A simple, physics-motivated machine- and electronics-shop project for university students," Am. J. Phys. **85**(12), 948–958 (2017).
[12]M. G. Bagliesi, C. Avanzini, G. Bigongiari, R. Cecchi, M. Y. Kim, P. Maestro, P. S. Marrocchesi, and F. Morsani, "A custom front-end ASIC for the readout and timing of 64 SiPM photosensors," Nucl. Phys. B-Proc. Sup. **215**(1), 344–348 (2011).
[13]Stéphane Callier, Christophe Dela Taille, Gisèle Martin-Chassard, and Ludovic Raux, "EASIROC, an easy & versatile readout device for SiPM," Physcs. Proc. **37**, 1569–1576 (2012).
[14]Marvin Weber Stephen Derenzo, Martin Boswell, and Kathleen Brennan, "Scintillation properties," a web page maintained by researchers at Lawrence Berkeley National Laboratory with the stated intention "to provide the measured scintillation properties of many inorganic materials, and citations to the published papers in which the measurements were reported." <http://scintillator.lbl.gov/>.
[15]P. Yang, C. D. Harmon, F. P. Doty, and J. A. Ohlhausen, "Effect of humidity on scintillation performance in Na and Tl activated CsI crystals," IEEE Trans. Nucl. Sci. **61**(2), 1024–1031 (2014).
[16]K. Pauwels, E. Auffray, S. Gundacker, A. Knapitsch, and P. Lecoq, "Effect of aspect ratio on the light output of scintillators," IEEE Trans. Nucl. Sci. **59**(5), 2340–2345 (2012).
[17]M. Grodzicka, M. Moszynski, T. Szczesniak, M. Szawlowski, D. Wolski, and J. Baszak, "MPPC array in the readout of Csi:Tl, LSO:Ce:Ca, $LaBr_3$:Ce, and BGO scintillators," IEEE Trans. Nucl. Sci. **59**(6), 3294–3303 (2012).
[18]P. R. Menge, K. Yang, M. McLaughlin, and B. Bacon, "Efficient positioning of silicon photomultipliers on large scintillation crystals," in *Proceedings of the 2016 IEEE Nuclear Science Symposium, Medical Imaging Conference and Room-Temperature Semiconductor Detector Workshop (NSS/MIC/RTSD)*, Strasbourg, France, (2016) pp. 1–5.
[19]M. Grodzicka, M. Moszynski, T. Szczesniak, M. Kapusta, M. Szawłowski, and D. Wolsk, "Energy resolution of scintillation detectors with sipm light readout," in *Proceedings of the IEEE Nuclear Science Symposium & Medical Imaging Conference*, Knoxville, TN (2010), pp. 1940–1948.
[20]P. Horowitz and W. Hill, *The Art of Electronics*, 3rd ed. (Cambridge U.P., New York, 2015), p. 254.
[21]F. Olschner (Cremat Inc.), Private Communication, 2017.
[22]Analog Devices AD8034 Datasheet Rev. D, Fig. 55, <http://www.analog.com/en/products/amplifiers/operational-amplifiers/jfet-input-amplifiers/ad8034.html>.
[23]C. F. G. Delaney and A. M. Lamki, "Long-lived phosphorescent components in NaI(Tl) and CsI(Tl)," Int. J. Appl. Radiat. Is. **19**(2), 169–170 (1968).
[24]P. Dorenbos, J. T. M. de Haas, and C. W. E. van Eijk, "Non-proportionality in the scintillation response and the energy resolution obtainable with scintillation crystals," IEEE Trans. Nucl. Sci. **42**(6), 2190–2202 (1995).
[25]W. W. Moses, G. A. Bizarri, R. T. Williams, S. A. Payne, A. N. Vasil'ev, J. Singh, Q. Li, J. Q. Grim, and W. S. Choong, "The origins ofscintillator non-proportionality," IEEE Trans. Nucl. Sci. **59**(5), 2038–2044 (2012).
[26]John D. Valentine, William W. Moses, Stephen E. Derenzo, David K. Wehe, and Glenn F. Knoll, "Temperature dependence of CsI(Tl) gamma-ray excited scintillation characteristics," Nucl. Instrum. Meth. A **325**(1), 147–157 (1993).
[27]F. Pennazio, G. Ambrosi, M. G. Bisogni, P. Cerello, F. Corsi, A. Del Guerra, M. Ionica, N. Marino, C. Marzocca, M. Morrocchi, C. Peroni, G. Pirrone, C. Santoni, and R. Wheadon, "Sipm-based pet module with depth of interaction," in *Proceedings of the 2012 IEEE Nuclear Science Symposium and Medical Imaging Conference Record (NSS/MIC)*, Anaheim, California (2012), pp. 3786–3789.
[28]United States Environmental Protection Agency (EPA), "RadTown USA" an educational website with specific sections regarding radioactive antiques, <https://www3.epa.gov/radtown/antiques.html>.
[29]Gavin K. Gillmore, Robin Crockett, Tony Denman, Alan Flowers, and Richard Harris, "Radium dial watches, a potentially hazardous legacy?," Environ. Int. **45**, 91–98 (2012).
[30]J. F. Mercier, B. L. Tracy, R. d'Amours, F. Chagnon, I. Hoffman, E. P. Korpach, S. Johnson, and R. K. Ungar, "Increased environmental gamma-ray dose rate during precipitation: a strong correlation with contributing air mass," J. Environ. Radioactiv. **100**(7), 527–533 (2009).
[31]B. Seitz, N. Campos Rivera, R. Gray, A. Powell, and F. Thomson, "Radiation sensors for medical, industrial and environmental applications: how to engage with schools and the general public," Phys. Educ. **53**(1), 014001 (2018).
[32]Eckert & Ziegler, a supplier of radioactive isotopes, maintains a website of recommended nuclear decay data, <http://www.ezag.com/home/products/isotope_products/isotrak_calibration_sources/general_technical_information/nuclear_decay_data/>. The "Lund/LBNL Nuclear Data Search" website is another valuable resource, S. Y. F. Chu, L. P. Ekström, and R. B. Firestone, <http://nucleardata.nuclear.l-u.se/toi/>.
[33]See Supplementary Material at https://doi.org/10.1119/1.5026595 for the basic Arduino UNO sketch.